Strength and compressional wave velocity variation in carbon dioxide hydrate bearing ottawa sand

Carlos Ordonez, Jocelyn L.H. Grozic
University of Calgary, Calgary, Alberta, Canada
Department of Civil Engineering– University of Calgary, Calgary, Alberta, Canada

ABSTRACT
This paper investigates the effects of carbon dioxide hydrate on the compressional wave (P-wave) velocity and shear strength of 20/30 and F110 Ottawa sand specimens under two different stress conditions. Gas hydrates were formed in partially water-saturated sand (20% saturation) at 36% porosity. The samples were isotropically consolidated to 0.95 and 1.35 MPa, then cooled to low temperatures (5°C) and finally axial stress was increased to achieve 3 MPa effective vertical stress. P wave variations were recorded at all testing stages, including during gas hydrate formation. The P wave velocities increased as temperature decreased, increased slightly with increasing anisotropy, increased during hydrates formation and shearing. The shear strength and stiffness was increased due to the presence of gas hydrates; friction angle was unaffected while an apparent cohesion was observed.

RESUMEN
el presente artículo presenta la variación de la velocidad compresional (P-wave) y resistencia al esfuerzo cortante de muestras de arena de Ottawa 20/30 y F110, en presencia de hidratos de dióxido de carbono. Los hidratos de gases fueron formados con la arena parcialmente saturada (20%) y a una porosidad de 36%. Las muestras fueron consolidadas isotrópicamente a 0.95 y 1.35 Mpa, enfriadas (5 grados Celsius), y finalmente el esfuerzo axial fue aumentado hasta alcanzar 3 Mpa de esfuerzo efectivo vertical. La variación en la velocidad compresional fue registrada en todas las etapas de los experimentos, así como también durante la formación de los hidratos de gas. La velocidad compresional aumentó cuando la temperatura disminuyó, en menor cantidad también aumentó cuando se aumentó la anisotropía, aumentó también cuando los hidratos de gases se formaron así como cuando las muestras se sometieron a esfuerzo cortante. La resistencia al esfuerzo cortante y la rigidez se aumento con la presencia de hidratos de gases; el ángulo de fricción no fue afectado pero una aparente cohesión fue observada.

1 INTRODUCTION

Natural gas hydrates consists of gas (mostly methane) trapped within a lattice of water molecules. Low temperature and high pressures are required for hydrates to stabilize similar to the conditions found in permafrost areas at high latitudes, in oceans and lake-bottoms.

Characterization of these compounds plays an important role when dealing with stability of the seafloor and submarine slopes and for evaluating seafloor stability over larger length scales (Nixon & Grozic 2006) for drilling and coring operations.

In this paper the influence of hydrates on the physical properties of Ottawa 20/30 sand samples is presented. The samples were prepared at 20% water saturations, both with and without CO_2 hydrates and then sheared at two different effective stresses (0.95 MPa and 1.35 MPa). During shearing compressional (P) wave velocities were recorded at different stages of the process. In order to provide a comparison between P-wave analyses on hydrate bearing sands, samples, both partially saturated and CO_2 hydrate bearing, were formed using Ottawa F110 sand (Waite et al. 2011). Again, P-wave velocity measurements were taken at different stages of the process.

The aim of this paper is to analyze the influence of the presence of hydrates on the strength and stiffness of Ottawa sand, using shear testing and P wave velocities, and to examine these properties with two different sand gradations.

2 EXPERIMENTAL PROGRAM

The tests were performed in Ottawa sand F110 and 20/30 samples; the grain size distribution of these sands is illustrated in Figure 1. F110 sand is fine sand which contains trace silt, while 20/ 20/30 Ottawa sand is medium in grain size and uniformly graded. All samples were tested at initial porosity of 36 ± 1%.

Samples from each material were tested at 20% water saturation, with and without hydrates, and at two effective pressures (1.35 MPa and 0.9 MPa). Table 1 summarizes the experimental program followed, in the hydrate column the "y" and "n" indicates if the sample contained hydrates or not respectively. During every test, P wave velocities were measured and the influence of particle size and distribution on the P wave was analyzed.

Table 1. Experimental program

Test	Sand type	Hydrate (yes or no)	Effective stress (MPa)
1	f110	no	1.35
2	f110	yes	1.35
3	20/30	no	1.35
4	20/30	no	0.90
5	20/30	yes	1.35
6	20/30	yes	0.90

Carbon dioxide hydrate has structure I, and assuming ideal filling of the cages, structure I hydrates have a molecular proportion of guest*5.75 H_2O ratio per each hydrate molecule (Dvorkin, et al. 2000) at 5°C , the density of H_2O is 0.999 g/cm^3, carbon dioxide is 0.85 g/cm^3 and the molecular weights of H_2O and CO_2 are 18.02 g/mol and 44.1 g/mol, respectively. One mole of carbon dioxide hydrate (if all cages are filled) has 37.48 g of CO_2 per 103.615 g of H_2O, which yields in a weight ratio H_2O/CO_2 of 2.92. The samples for the present study were prepared at 20% water saturation, the weight of water in each sample for approximately 36% porosity is approximately 15.5 g. Using weight to weight ratio, and assuming all water will form hydrate, the weight of CO_2 that form hydrates would be 5.3 g, which results in 20.8 g of carbon dioxide hydrate. Carbon dioxide hydrate density is 1.1 g/cm^3 (Aya et al. 1997), thus using this density, each sample has 18.95 cm^3 of carbon dioxide hydrate approximately, which is around 25 % hydrate saturation (void occupancy).

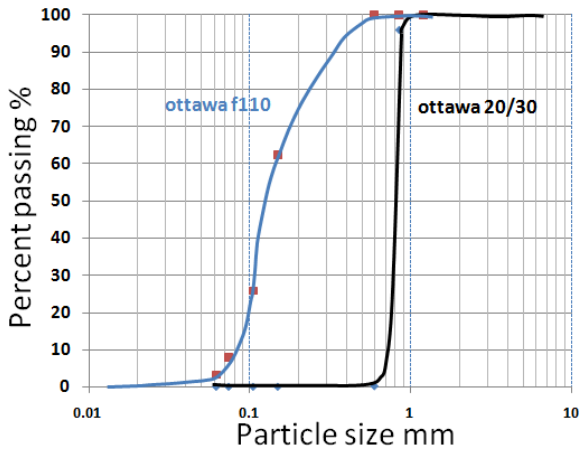

Figure 1. Particle size distribution of Ottawa sand 20/30 and Ottawa sand F110

2.1 Testing Instrumentation

The tests were carried out on a high pressure triaxial apparatus adapted with a temperature control system and an ultrasonic (for P-wave and S-wave measurements) device, see Figure 2. Temperature control is achieved through circulation of refrigerant through two copper tubes which are spiralled around the inside wall of the cylindrical cell. The cell oil surrounding the sample is cooled which subsequently cools the sample. The temperature is controlled using two thermistors located close to the sample as illustrated in Figure 2. Additional temperature measurements are recorded at the pore fluid connection at the base of the triaxial cell. Accuracy of the temperature control system is ± 1°C.

Housed within the top and bottom platens are a set of piezo-electric P and S crystals. A wave form is generated at the sample base and measured at the sample top, and for a given sample length (monitored with a linear voltage displacement transducer), the wave velocity can be calculated from Eq. 1:

$$V = \frac{l}{t - t_0,} \qquad [1]$$

where t is the arrival time of a particular waveform feature, and t_o is the first arrival time of that same waveform feature when the transducer endcaps are in contact with each other in the absence of a specimen.

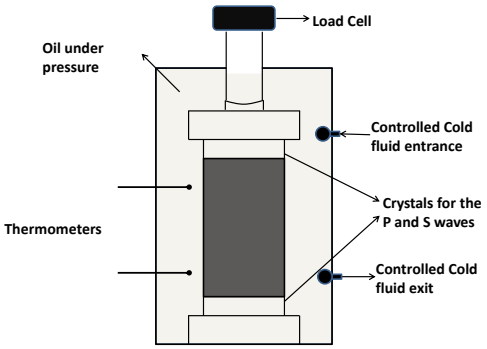

Figure 2. Temperature controlled triaxial schematic

2.2 Sample Preparation and hydrate formation method

After attaching the bottom platen to the base of the cell, sample fabrication begins in each case by weighing room-dry (F110, 20/30) sand. Distilled water is added to the sand and mixed in a plastic bowl by hand for 3-5 minutes. The mass of added water is calculated based on the 370g mass of sand for the F110 and 390g mass for the 20/30 Ottawa sand, with 20% water-saturation of the pore space; the specific gravity of sand is 2.65.

A flexible neoprene membrane (0.3 mm thickness) is stretched over the bottom platen and a split mold assembled around the membrane. A nominal vacuum supply is used to keep the membrane taunt to the mold. For each sample type, about 50 g sand is placed into the mold and tamped by hand with an 1125 g, 40 mm-diameter steel compactor. The membrane is then assembled around the sample, a vacuum applied to the sample bottom (~25 kPa), and the split mold removed. 0-rings keep the membrane securely attached to the top and bottom pedestals. At this point sample diameter and height measurements are taken to determine initial sample dimensions. The triaxial cell wall is then lowered and the cell filled with oil.

A nominal "seating" deviator stress is applied (~10 kPa) to ensure the piston is in contact with the sample top cap. Cell pressures are then increased to 400kPa and the sample vacuum released.

Increasing the effective confining pressure to 1.35 MPa at room temperature then isotropically consolidates the sample. For F110 sand samples, the pore pressures remained at atmospheric and the deviator stress was increased slowly to 1.65 MPa resulting in a vertical effective stress of 3 MPa. The sample was then cooled to 5°C over the course of approximately 0.5 hours; it was then left to equilibrate for many hours.

For the hydrate-bearing Ottawa F110 sample(s), first carbon dioxide gas was flushed through the sample to replace the air at the nominal confining pressure of 25 to 50 kPa. The sample was then isotropically consolidated to 1.35 MPa, with no pore pressures, at room temperature. At this stage, carbon dioxide gas was introduced and the gas pressure and confining pressure incrementally and gradually increased at the same rate to 3.95 MPa and 5.30 MPa, respectively, to maintain an effective confining pressure of 1.35 MPa. The sample was then cooled to 5°C to initiate gas hydrate formation. Cooling occurred over approximately 0.5 hours, and then the sample was left to equilibrate for approximately 6 hours. At this point, the deviator stress was increased to 1.65 MPa and the sample left for another 16 hours for hydrate formation. For the hydrate-bearing Ottawa 20/30 samples the procedure was the same as the F110 sand, with the addition of drained shearing after hydrate formation.

3 STRENGTH AND DEFORMATION

Waite et al. (2009) have shown that the presence of methane hydrate increases stiffness, enhances prefailure dilation, and leads to higher strength. Although carbon dioxide was used as the hydrate former in this study, the hydrates exhibit same structure as methane hydrates (structure 1), and thus it is anticipated that strength properties are not influenced by the gas composition to a large extent.

3.1 Laboratory Measurements

Confined drained triaxial tests were performed on samples 3, 4, 5 and 6 (Table 1). Table 2 summarize the peak strength found for each of the samples.

Table 2. Drained confined triaxial test results for Samples 5, 6, 7 and 8

Test	Hydrate (yes or no)	Effective stress (MPa)	Peak stress (MPa)
3	no	1.35	3.4
4	no	0.95	2.37
5	yes	1.35	4.55
6	yes	0.95	3.35

It was observed that the strength of the sample significantly increases when hydrates are present. Results obtained at different effective confining stress levels have been combined to define the linear Coulomb failure envelope from which strength parameters are derived (Figure 3).

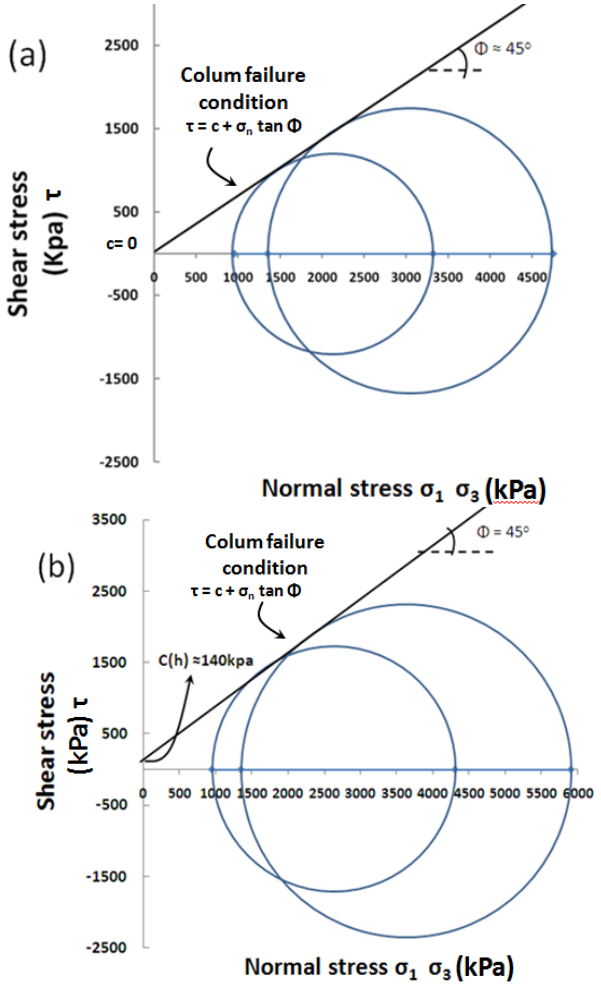

Figure 3. Mohr circle for 20/30 sand (a) without hydrates (Samples 3 &4) and (b) with hydrates (Samples 5 & 6)

A friction angle of 45° was obtained for both envelops (with and without hydrates). It was observed in Figure 3a that, the moist sand samples exhibited no cohesion as the failure envelope passed through intercept where cohesion is zero, but the hydrate bearing samples developed an apparent cohesion of approximately 140 kPa. This cohesion for samples with hydrates is the result of cementation of the sand grains which results in an increase in strength.

From the stress strain curves, shown in Figure 4, an increase in dilatancy in the hydrate samples is observed, relative to the moist sand samples, which can be attributed to the hydrate cementation. The material stiffness can be measured by obtaining the secant modulus of the early portion of the stress strain curve (0 to 1 % strain); greater stiffness was observed for the hydrate bearing samples. Figure 5 shows the Young's modulus at 50% of deviator stress at failure (with failure defined as when constant volume is achieved or 15% strain) for each sample. It was observed that for both effective confining pressures, the Young's modulus differs by approximately 200 MPa between the hydrated and moist samples. These values are in agreement with previous results for cemented sand at low hydrate saturation (see Waite et al. 2009, Winters et al. 2006)

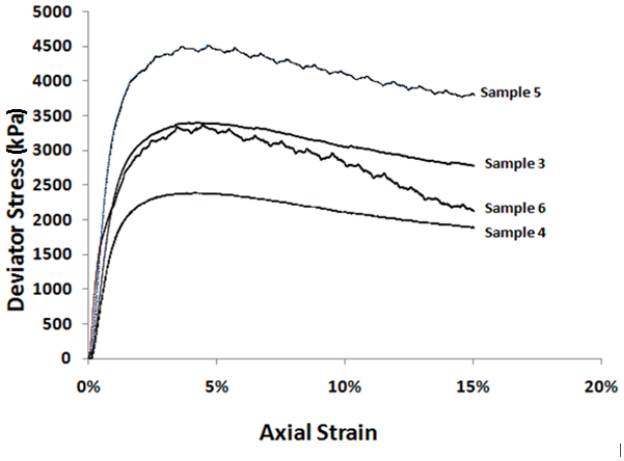

Figure 4. Stress strain curves for Samples 3, 4, 5 and 6

4 COMPRESSIONAL WAVE VELOCITY

The ultrasonic measurement program was designed to characterize the dynamic response of F110 sand specimens containing CO_2 gas hydrate within the pore space under isotropic and anisotropic loading. Compressional wave measurements were taken at different stages in the formation process to determine the effect of hydrate formation on the physical response.

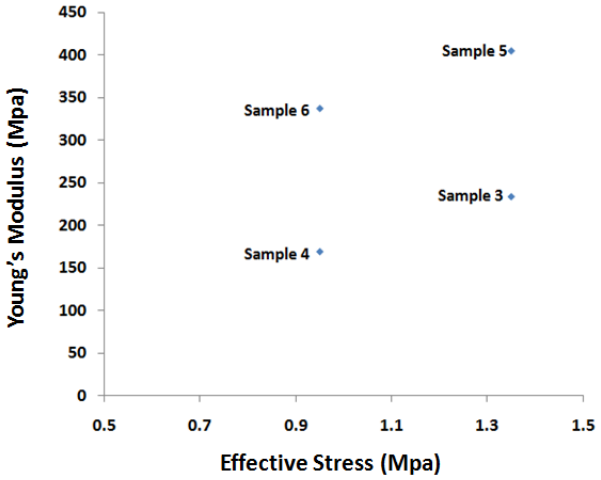

Figure 5. Young's Modulus vs effective confining stress

4.1 Ultrasonic Measurements for F110 Ottawa Sand

Table 3, describes the stages at which the P-wave velocities were measured. For moist samples, without hydrates, no back pressure was applied, while back pressure was required for the hydrate bearing samples. Steps 1, 2, 3 and 4 are for Sample 1 with no hydrates, the variation in these tests are the increase of deviator stress until Step 3 and the difference between step 3 and 4 is the change in temperature from 14 to 5°C. Steps 5, 6, 7, and 8 are applicable to Sample 2 (hydrate bearing sample), in these steps back pressure was applied to form hydrates, and in Step 8 the ideal temperature pressure condition for hydrate growth is achieved by reducing the temperature and the sample is left to equilibrate for 16 hours. For Sample 2, P-wave measurements were obtained throughout the hydrate forming process; measurements were taken for about 16 hours, with the readings commencing once the sample was within the hydrate formation pressure and temperature zone. Figure 6 illustrates the increase in P wave velocity as hydrate formation occurs.

P-wave velocities were influenced by the stress state of the soil. Table 4 shows the P-wave velocity for each of the steps and the influence of hydrate content and state of stresses can be observed. Figure 7 shows the variation of P-wave velocity, as the deviator stress increased, so did the P-wave velocity. Prior to hydrate formation, the Samples 1 and 2 have virtually the same P-wave velocity as expected; once hydrate forms in Sample 2, the velocity is increased significantly in that sample.

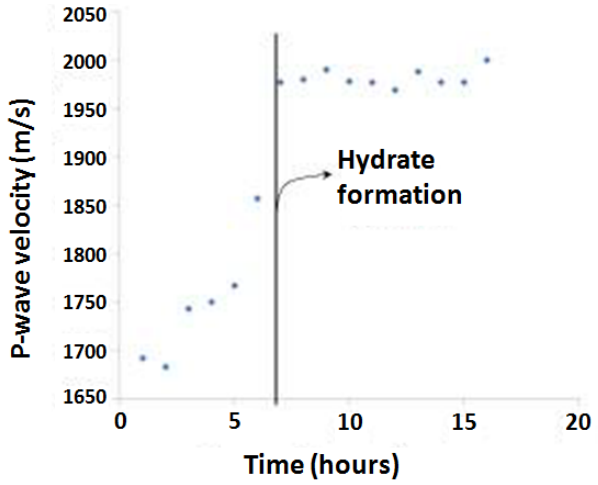

Figure 6. P-wave velocities vs time during hydrate formation for Sample 2

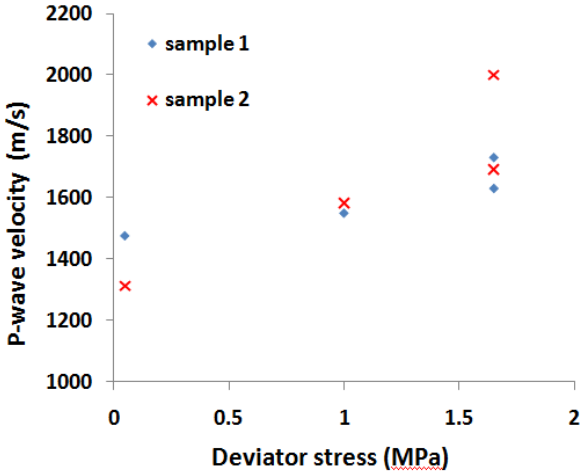

Figure 7. Variation of P-wave velocity as deviator stress is increased for Samples 1 and 2. [change capitals in figure of Sample 1 and 2]

Table 3. Stages of the testing in F110 Ottawa sand

Stage	Confinement Pressure (MPa)	Back Pressure (MPa)	Temp. (°C)	Deviator Stress (MPa)
1	1.35	0	14	0.05
2	1.35	0	14	1.00
3	1.35	0	14	1.65
4	1.35	0	5	1.65
5	5.30	3.95	14	0.05
6	5.30	3.95	15	1.00
7	5.30	3.95	15	1.65
8	5.30	3.95	5	1.65

Table 4. P-wave velocity measurements for F110 samples

Step	Sample 1 (m/s)	Sample 2 (m/s)
1	1476	1450
2	1550	N/A
3	1631	N/A
4	1732	N/A
5	N/A	1313
6	N/A	1583
7	N/A	1692
8	N/A	2000

Values obtained in this program (1476-2000 m/s) are in agreement with those published for methane hydrate bearing sands (e.g. Waite et al. 2009, Priest et al. 2005) but are lower than those reported in the recent international gas hydrate laboratory comparison project (Waite et al. 2011).

4.2 Ultrasonic measurements for 20/30 Ottawa sand

P-wave velocity measurements in 20/30 Ottawa sand, under the stages as described previously, with the addition of Step 9, which is at the point of failure (at ultimate shear stress at approximately 15% strain). The results are presented in Table 5 and Figure 8.

Table 5. P-wave velocity measurements for Samples 3, 4, 5 and 6.

Stage	Sample3 (m/s)	Sample4 (m/s)	Sample5 (m/s)	Sample6 (m/s)
1	1780	1888	1970	1398
2	1801	N/A	N/A	N/A
3	1850	1890	N/A	N/A
4	1909	1915	N/A	N/A
5	N/A	N/A	2057	1805 *
6	N/A	N/A	2057	1908 *
7	N/A	N/A	2057	2015*
8	N/A	N/A	2507	2447*
9	2668	2399	3313	3200*

* In Sample 6 confinement was 4.8MPa and back pressure was 3.9 MPa

For Sample 6 P-wave measurements were taken during the formation process, but at constant pressure and temperature, with time being the only variable. Measurements were taken for about 20 hours, until it was ensured hydrate had formed; the results are illustrated in Figure 9. Similar to the F110 sand, once formation commences, the P-wave rapidly increases.

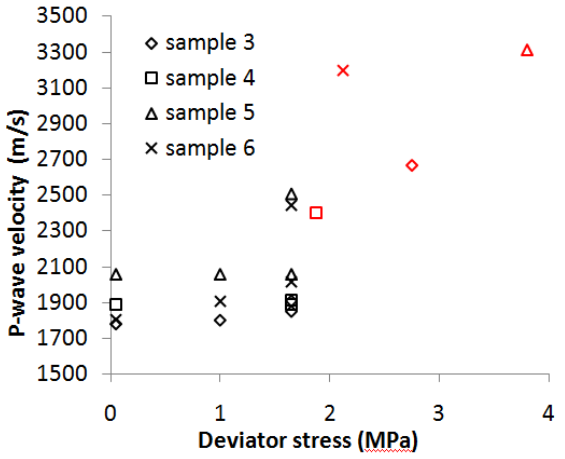

Figure 8. Variation of P- wave velocity as deviator stress is increased for Samples 3, 4, 5, and 6. Points in red are the P-wave velocities at failure

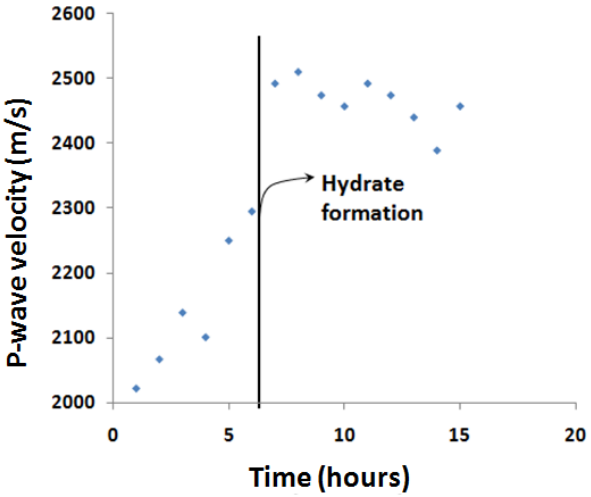

Figure 9 P-wave velocities vs time during hydrate formation for Sample 6

4.3 Comparison of P-wave results for F110 and 20/30 Ottawa sand

In the present study it has been shown that P-wave velocities for 20/30 Ottawa sand were higher than those for F110 sand. The difference in the P-wave velocities can be explained on the basis of the difference in grain size and grain size distribution of the two types of sand (Figure 1). Ottawa 20/30 not only has larger particles than F110 sand but it is also more uniformly graded which results in a larger diameter of the interconnected void paths for the 20/30 Ottawa sand compared to F110. As the interconnected void paths in F110 Ottawa samples are smaller, capillarity and narrow void spaces may play an important role in the uniformity of the hydrate formation (Clennell et al. 1999). A better distribution of the hydrates for the 20/30 Ottawa samples, may be the main reason for higher P-wave velocities compared to those of F110 Ottawa samples.

It is also important to note that the same amount of water was used for both type of sand samples but since the F110 sand samples have a larger surface area, the hydrate film that coats the sand grain would, theoretically, be thinner in the F110 sand compared to 20/30 Ottawa sand. This thinner hydrated film would decrease cementation for the F110 samples resulting in lower P-wave values (see Figure 10).

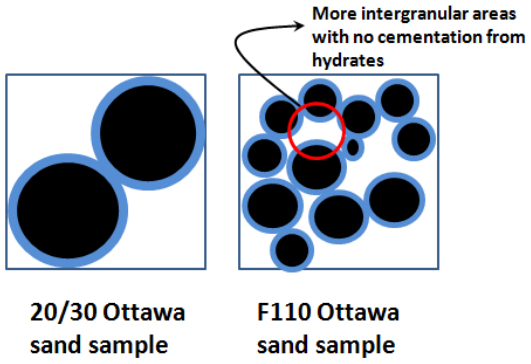

Figure 10. Illustration of surface area difference between F110 and 20/30 Ottawa sand

5 CONCLUSIONS

The presence of carbon dioxide hydrates within sand samples (Ottawa 20/30) increased the sand strength and stiffness, by 70% and 74% for the effective confining stresses of 0.95 and 1.35 MPa, respectively. The stiffness, measured by Young's Modulus, increased by 200 MPa in the presence of hydrates for both effective confining stresses.

It was concluded that the time required for hydrate formation was similar for both sands, approximately 7 hours as shown by the response depicted by P-waves. The P-wave velocities increased due to formation of gas hydrates within the pore spaces. The velocities were significantly higher for Ottawa 20/30 sand than for F110 sand. Ottawa 20/30 sand is uniformly graded coarse sand, and thus has large pore spaces which reduces capillary pressures and eases hydrate formation. On the other hand, F110 sand is finer, with a wider range of grain size distributions, including some silt content, the

resulting smaller void spaces create capillary and hydrate formation can be inhibited in certain locations. For all Ottawa sand samples there was a significant increase in the P-wave velocity after shear, this is because as the carbon dioxide gas was expelled from the sample during drained shear, the void spaces were reduced thus increasing the stiffness, or contact areas, which is reflected in a higher P-wave velocity.

F110 Ottawa sand better simulates natural marine sediments hosting hydrates, which are often fine-grained, where the narrow pore size condition can inhibit hydrate growth in certain areas (Andersonet al. 2009). 20/30 Ottawa sand also simulates natural conditions for coarser marine or terrestrial sediments, with larger pore size and more uniform gradation. Results from the study presented in this paper illustrate that even a modest quantity of hydrate will increase the soil strength and stiffness which is an important observation for analyzing seafloor stability or initial hydrate reservoir conditions

ACKNOWLEDGEMENTS

The author's gratefully acknowledge the financial contributions of NSERC (Natural Sciences and Engineering Research Council of Canada) and NRC (Natural Resources Canada; Geological Survey of Canada).

REFERENCES

Anderson, R., Tohidi, B., & Webber, J. (2009). Gas hydrate growth and dissociation in narrow pore networks: Capillary inhibition and hysteresis phenomena. *Journal of Geological Society Special Publication* , 145-159.

Aya, I., Yamane, K., & Narai, H. (1997). Solubility of CO2 and density of CO2 hydrate at 30 MPa. *International Symposium on CO2 Fixation and Efficient Utilization of Energy* (pp. Pages 263-271). Elsevier Science Ltd.

Clennell, M., Hovland, M., Booth, J., & Winters, W. (1999). Formation of natural gas hydrates in marine sediments. Part 1: Conceptual model of gas hydrate growth conditioned by host sediment properties. *Journal of Geophysical Research* .

Dvorkin, J., Helgerud, M., Waite, W., Kirby, S., & Nur, A. (2000). Introduction to physical properties and elasticity models . In *Natural Gas Hydrate In Oceanic and Permafrost Environments* (pp. 245-260). dordrecht, Netherlands: kluwer academic publishers.

Nixon, M. F., & Grozic, J. L. (2006). A simple model for submarine slope stability analysis with gas hydrates. *Norwegian Journal of Geology , 86*, 309-316.

Priest, J. A., Best, A. I., & Clayton, C. R. (2005). A laboratory investigation into the seismic velocities of methane gas hydrate-bearing sand. *Journal of Geophysical Research* .

Waite, W., Santamarina, J., Chong, S., Grozic, J., Hester, K., Howard, et al. (2011). Inter-laboratory comparison of wave velocity measurements in a sand under hydrate-bearing and other set conditions. *7th international conference on gas hydrates.*

Waite, W., Santamarina, J., Cortes, D., Dugan, B., Espinoza, D., Germaine, J., et al. (2009). Physical properties of hydrate-bearing sediments. *Journal of American Geophysical Union* .

Winters, W., Waite, W., Mason, D., Gilbert, L., & Pecher, I. (2006). Methane gas hydrate effect on sediment acoustic and strength properties. *Journal of Petroleum Science and Engineering* , 127-135.

Zhang, W., Durham, W. B., & Kirby, S. H. (2002). The strength and rheology of methane clathrate hydrate. *Journal of Geophysical Research* .